IEEE Photonics Journal
An IEEE Photonics Society Publication

Bias Switchable Dual-Band InAs/GaSb Superlattice Detector With pBp Architecture

Volume 3, Number 2, April 2011

E. A. Plis
S. S. Krishna
N. Gautam
S. Myers
S. Krishna, Senior Member, IEEE

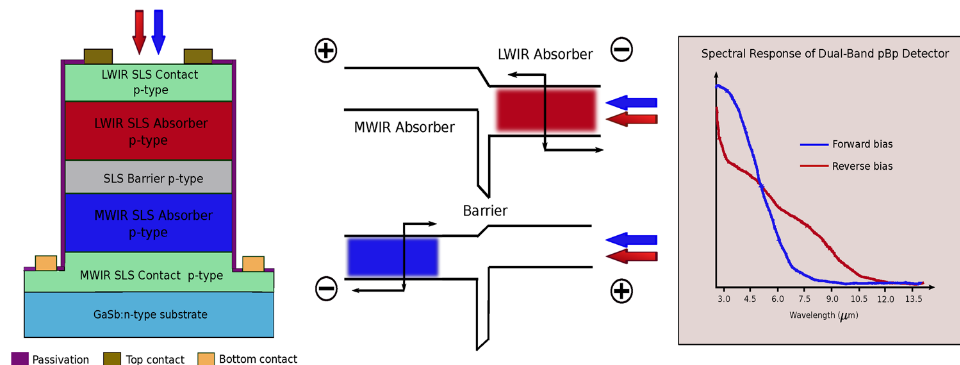

DOI: 10.1109/JPHOT.2011.2125949
1943-0655/$26.00 ©2011 IEEE

IEEE photonics SOCIETY
IEEE

Bias Switchable Dual-Band InAs/GaSb Superlattice Detector With pBp Architecture

E. A. Plis,[1,2] S. S. Krishna,[1] N. Gautam,[2] S. Myers,[2] and S. Krishna,[1,2] *Senior Member, IEEE*

[1]SK Infrared, LLC, Lobo Venture Lab 801, Albuquerque, NM 87106 USA
[2]Center for High Technology Materials, Department of Electrical and Computer Engineering, University of New Mexico, Albuquerque, NM 87106 USA

DOI: 10.1109/JPHOT.2011.2125949
1943-0655/$26.00 ©2011 IEEE

Manuscript received February 3, 2011; revised February 28, 2011; accepted March 1, 2011. Date of publication March 10, 2011; date of current version March 25, 2011. This work was supported by the Navy SBIR Phase I Contract N68936-10-C-0080. Corresponding author: E. A. Plis (e-mail: elena.plis@gmail.com).

Abstract: We report on a dual-band [mid/long-wave infrared (MWIR and LWIR)] InAs/GaSb strained layer superlattice detector with a pBp architecture. Fifty percent cutoff wavelengths of 5 and 9 μm were obtained with diffusion-limited behavior for midwave IR absorber. At 77 K, the peak D* values were equal to 5×10^{11} Jones $(V_b = +0.1\ \text{V}, \lambda = 5\ \mu\text{m})$ and 2.6×10^{10} Jones $(V_b = -0.4\ \text{V}, \lambda = 9\ \mu\text{m})$. The corresponding values of responsivity and quantum efficiency were 1.6 A/W and 39% (MWIR) and 1.3 A/W and 17% (LWIR).

Index Terms: Optoelectronic materials, nanostructures, InAs/GaSb strained layer superlattices (SLS).

1. Introduction

Multicolor detection, along with high operation temperature and large format arrays, are the characteristics of the third generation of infrared (IR) imaging systems. Data collection in separate IR bands is highly beneficial for military and civil applications involving identification of temperature differences and determination of the thermal characteristics of an object. Detectors based on interband [Mercury–Cadmium–Telluride (MCT)] and intersubband [quantum well infrared detectors (QWIPs)] transitions have been the dominant technologies for such applications [1], [2].

Difficulties in the epitaxial growth of MCT and low electron effective mass $(0.009\ m_o)$ resulting in large dark current due to tunneling especially at longer wavelengths [3] affect the development of multispectral cameras based on MCT. With respect to MCT detectors, QWIPs have a number of advantages, including the use of standard manufacturing techniques based on a mature GaAs growth and processing technologies, highly uniform and well-controlled MBE growth on larger area GaAs wafers (6 in.), high yield and, thus, low cost, and more thermal stability. However, they have larger dark currents and lower quantum efficiencies compared with the interband devices. On the contrary, the basic material properties of InAs/GaSb type-II strained layer superlattices (SLS) provide a prospective benefit in the realization of dual-color imagers. The strain in InAs/GaSb type-II SLS system facilitates suppression of interband tunneling [4] and Auger recombination [5] processes. Moreover, the larger effective mass in SLS leads to a reduction of tunneling currents compared with MCT detectors of the same bandgap. By optimizing the oscillator strength in this material system, a large quantum efficiency and responsivity can be obtained.

Despite the prominent advantages of SLS technology, only a few reports of dual-band detectors based on InAs/GaSb SLS have been published so far. The dual-color SLS cameras [MWIR (4 μm)/

MWIR (5 μm) and MWIR (7.7 μm)/LWIR (10 μm)] possess a vertical detector design based on two back-to-back InAs/GaSb SLS photodiodes separated by a common ground contact layer [6], [7]. These detectors are based on conventional p-i-n design which is characterized by high diffusion and Shockley–Read–Hall (SRH) generation-recombination dark currents. Moreover, they require multiple contacts per pixel resulting in a complicated processing scheme and expensive specific read-out circuits. The MWIR/LWIR detectors based on nBn design [8], [9] are expected to reduce the dark current level due to elimination of depletion region in detector heterostructure. In addition, multicolor detectors with nBn design do not require multiple contacts per pixel, which reduces the cost and complexity associated with the FPA fabrication process.

Typical dual-band SLS detector with nBn design is composed by two narrow band-gap absorbers (n) the different IR regions separated by a 100-nm-thick wide-band-gap material layer with a large barrier for electrons and no barrier for holes (B). As a result, the majority carrier current between the two electrodes is blocked by the large energy offset, while there is no barrier for photogenerated minority carriers. However, photocarriers in this case are the low mobility holes. It would be desirable to have the inverted structure, (i.e., pBp detector) in which the photocarriers are the higher mobility electrons.

In this paper, we report a dual-band InAs/GaSb SLS detector with a pBp architecture. The dual-band pBp SLS detector has shown the shot noise limited detectivity at 77 K of 5×10^{11} Jones (at $\lambda = 5$ μm and $V_b = +0.1$ V) and 2.6×10^{10} Jones (at $\lambda = 9$ μm and $V_b = -0.4$ V) for MWIR and LWIR absorbers, respectively. The maximum values of quantum efficiency were estimated to 41% (MWIR absorber) and 25% (LWIR absorber) at $V_b = +0.4$ V and $V_b = -0.7$ V. The performance of the pBp detector is superior to that of previously reported dual-band (MWIR/LWIR) QWIP detectors and is comparable with that of dual-band MCT detectors in the MWIR band.

2. Experimental Details

The devices studied in this work were grown on the Te-doped epiready (100) GaSb substrate by a solid source MBE VG-80 system. The active region of pBp dual-band detector structure was formed by LWIR (14 ML InAs/7 ML GaSb:Be SLS, p-type) and MWIR (10 ML InAs/4 ML GaSb:Be SLS, p-type) absorbing regions with thicknesses of 2 μm separated by the 100-nm barrier (16 ML InAs/ 4 ML AlSb:Be SLS, $p = 1 \times 10^{16}$ cm^{-3}). The doping level of MWIR and LWIR absorbing regions was estimated as $p = 1 \times 10^{16}$ cm^{-3} based on GaAs equivalent.

Semiempirical pseudopotential method [10] integrated with a SENTAURUS TCAD simulation platform [11] was used for calculation of band lineup of LWIR and MWIR absorbing regions with the barrier. The energy band diagram of active region of pBp detector showing conduction band (CB) and valence band (VB) energies under zero, forward ($V_b = +0.1$ V), and reverse biases ($V_b = -0.1$ V) at 77 K is presented in Fig. 1. Special care was taken to minimize the conduction band offset for the unhindered movements of the photocarrier electrons between contacts. The designed conduction band offset was equal 9 meV.

Device fabrication was initiated with a standard optical photolithograpy to define 410 μm $\times$ 410 μm square mesa devices with apertures ranging from 25 to 300 μm. Etching was performed using inductively coupled plasma (ICP) reactor with BCl_3 gas. Resulting etch depth was 4.7 μm, which corresponds to the middle of the bottom contact layer of the detector. Next, ohmic contacts were evaporated on the bottom and top contact layers using Ti (500 Å)/Pt (500 Å)/Au (3000 Å) in both cases. Finally, devices were passivated by SU-8 2002 photoresist [12] after a short (40 s) dip in a phosphoric acid-based solution ($H_3PO_4 : H_2O_2 : H_2O = 1 : 2 : 20$) that is intended to remove native oxide film formed on the etched mesa sidewalls. The resulting thickness of SU-8 passivation film was 1.5 μm. The cross section of fabricated pBp dual-band detector is shown in Fig. 2.

3. Results and Discussion

The normalized spectral response of a pBp dual-band detector under different polarities of applied bias was measured at 77 K with a Fourier transform IR spectrometer (FTIR), as shown in Fig. 3. Under forward bias, which is defined as positive voltage applied to the top contact, the photogenerated

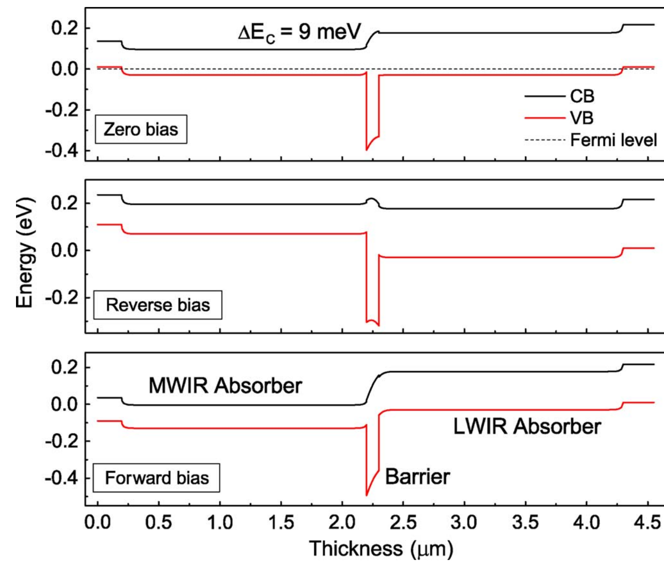

Fig. 1. Energy band diagram of pBp detector calculated at 77 K under zero (top), reverse (middle), and forward (bottom) biases.

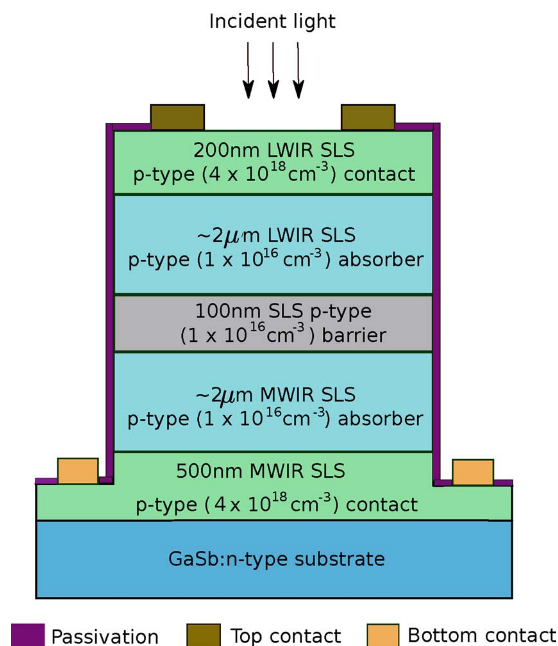

Fig. 2. Cross section of fabricated pBp dual-band detector.

carriers are collected from the MWIR absorber. When the device is under reverse bias, which is defined as negative voltage applied to the top contact, the photogenerated carriers from the LWIR absorber are collected, while those from the MWIR absorber are blocked by the barrier. Thus, a two-color response is obtained under two different bias polarities. The zero-response cutoff wavelengths $(\lambda_{100\%})$ of MWIR and LWIR absorbers were equal to 7.8 μm and 12.0 μm, respectively (77 K).

Current–voltage (*IV*) characteristics were measured for temperatures ranging from 30 to 300 K. Representative dark current density versus applied bias curve measured at 77 K for a 400 μm $\times$ 400 μm device is shown in Fig. 4. Fig. 5 shows the dark current density as a function

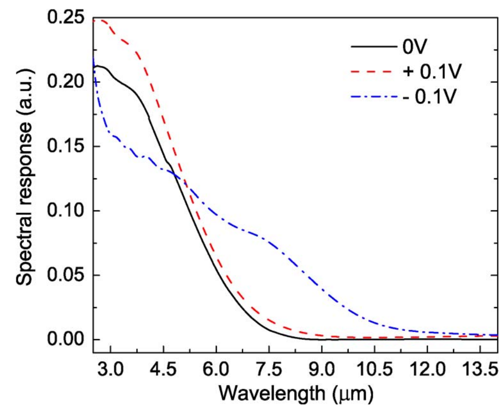

Fig. 3. Normalized spectral response of dual-band pBp detector measured at 77 K. MWIR and LWIR responses are observed under forward and reverse bias polarity, respectively.

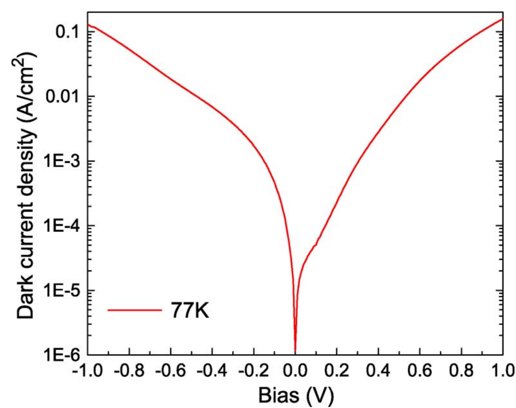

Fig. 4. Dark current density as a function of applied bias measured at 77 K.

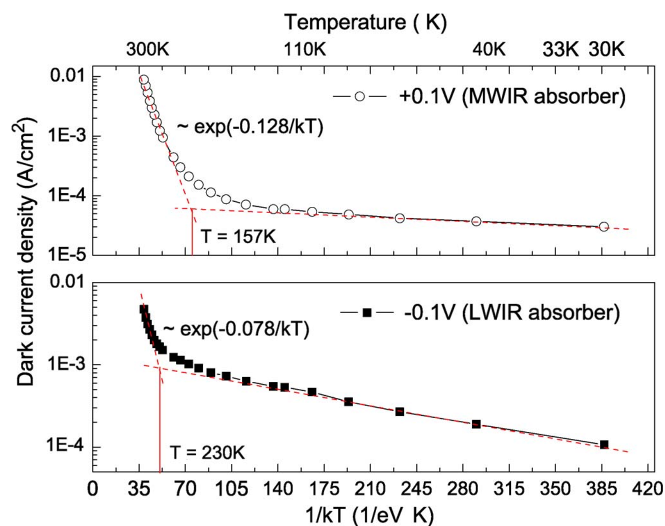

Fig. 5. Dark current density as a function of detector temperature measured for +0.1 V (MWIR absorber) and −0.1 V (LWIR absorber) of applied bias.

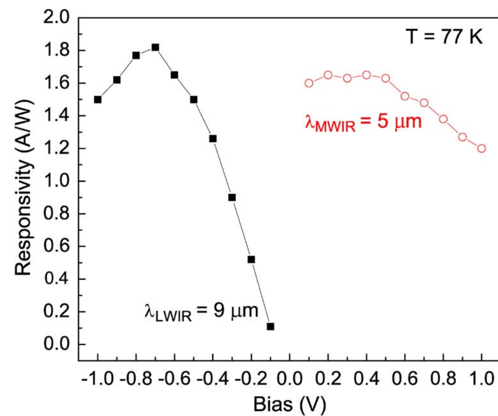

Fig. 6. Responsivity of pBp dual-band detector measured as function of applied bias.

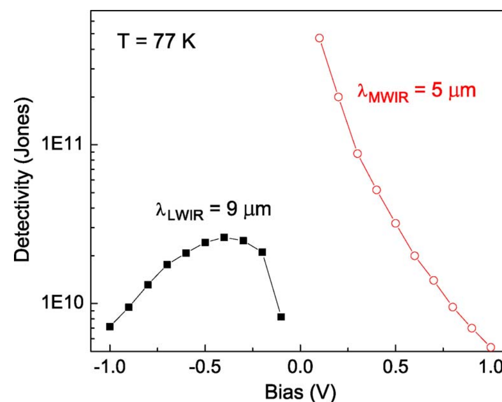

Fig. 7. Specific detectivity of pBp dual-band detector measured as function of applied bias.

of detector temperature measured at $+0.1$ V and -0.1 V of applied bias. At 77 K, the dark current density was equal to 6×10^{-5} A/cm^2 at $+0.1$ V (MWIR absorber) and 5×10^{-4} A/cm^2 at -0.1 V (LWIR absorber).

At high temperatures, the extracted activation energy of MWIR absorber (0.128 eV) is found to be very close to the nominal value of the optical band gap (0.159 eV). This behavior indicates that the current is dominated by a diffusion mechanism. The saturation observed at lower temperatures is probably due to the trap-assisted tunneling [13]. For the LWIR absorber, the value of activation energy at higher temperatures (0.078 eV) was proportional to the 2/3 Eg (0.103 eV), indicating that the LWIR absorber is limited by the SRH generation process.

The responsivity of dual-band pBp detector with an aperture of 100 μm was measured under a 2π field of view (FOV) with a calibrated blackbody source at 800 K. Fig. 6 shows the measured responsivity for MWIR and LWIR absorbers.

One of the concerns in multiband detectors is the spectral crosstalk. Ideally, the MWIR absorber should only respond for wavelengths below 7.8 μm, and the LWIR absorber should respond to wavelengths between 7.8 μm and 12 μm. However, the InAs/GaSb superlattice detectors are broadband detectors and are susceptible to spectral crosstalk; in other words, the LWIR absorber will detect all the radiation below 12 μm. We measured black body broadband responsivity and QE for the presented detector structure. In order to define the responsivity and QE at particular wavelengths, additional measurements need to be performed with set of narrow band filters. These measurements are currently being undertaken.

TABLE 1

Performance comparison of dual-band single element detectors based on InAs/GaSb SLS with pBp architecture, QWIP, and MCT

Parameter	MCT [14] [15]	QWIP [16] [17] [18]	SLS with pBp architecture
MWIR response, $\lambda_{50\%}$ *50% cut-off* (μm)	5	5.1	5
LWIR response, $\lambda_{50\% cut-off}$ (μm)	10	8.9	9
D* (Jones) (MWIR)	6×10^{11}	1×10^{11}	5×10^{11}
D* (Jones) (LWIR)	4×10^{12}	2×10^{10}	2.6×10^{10}
QE (%) (MWIR)	> 70	19	39
QE (%) (LWIR)	> 50	15	17

The shot noise limited D^* was evaluated at 5 μm and 9 μm for MWIR and LWIR absorbers, respectively, using the equation

$$D^* = \frac{R}{\sqrt{\frac{4k_B T}{R_d A_d} + 2qJ}} \tag{1}$$

where R is responsivity, k_B is the Boltzman constant, T is temperature, R_d is dynamic resistance, and A_d is diode area, q is the electronic charge, and J is the dark current density.

Values of specific detectivity at different temperatures are shown in Fig. 7. At 77 K, the peak D^* has reached 5×10^{11} Jones ($V_b = +0.1$ V, $\lambda = 5$ μm) and 2.6×10^{10} Jones ($V_b = -0.4$ V, $\lambda = 9$ μm). The corresponding values of responsivity and quantum efficiency were 1.6 A/W and 39% (MWIR) and 1.3 A/W and 17% (LWIR).

It should be noted that the detector is operated under small values of applied bias compared with nBn dual-band SLS detector [9], thus illustrating the advantages of the pBp design. Performance comparison of dual-band single element detectors based on InAs/GaSb SLS with pBp design, QWIP, and MCT is shown in Table 1. It should be noted that all the parameters in Table 1 are stated at $\lambda_{50\%\ \mathrm{cutoff}}$. The dual-band InAs/GaSb SLS detector with pBp design showed superior performance to the QWIP detectors both in MWIR and LWIR bands and comparable performance with MCT detectors in the MWIR band. Better performance of a dual-band HgCdTe detector in the LWIR band is attributed to the considerably thicker (10 μm) absorbing layer of MCT detector.

4. Conclusion

In conclusion, we have designed and demonstrated dual-band response from InAs/GaSb SLS detectors with a pBp architecture. Diffusion-limited behavior of dark current at higher temperatures was observed for MWIR absorber. At 77 K, the peak D^* has reached 5×10^{11} Jones ($V_b = +0.1$ V, $\lambda = 5$ μm) and 2.6×10^{10} Jones ($V_b = -0.4$ V, $\lambda = 9$ μm). The corresponding values of responsivity and quantum efficiency were 1.6 A/W and 39% (MWIR) and 1.3 A/W and 17% (LWIR).

Acknowledgment

The authors would like to thank the user service center at the University of New Mexico for sample fabrication and testing.

References

[1] D. F. King, J. S. Graham, A. M. Kennedy, R. N. Mullins, J. C. McQuitty, W. A. Radford, T. J. Kostrzewa, E. A. Patten, T. F. McEwan, J. G. Vodicka, and J. J. Wootan, “3rd-generation MW/LWIR sensor engine for advanced tactical systems,” *Proc. SPIE*, vol. 6940, pp. 69402R-1–69402R-12, Apr. 2008.

[2] A. Soibel, S. D. Gunapala, S. V. Bandara, J. K. Liu, J. M. Mumolo, D. Z. Ting, C. J. Hill, and J. Nguyen, “Large format multicolor QWIP focal plane arrays,” *Proc. SPIE*, vol. 7298, pp. 729 806–729 813, May 2009.

[3] A. Rogalski, "HgCdTe infrared detector material: History, status and outlook," *Rep. Progr. Phys.*, vol. 68, no. 10, pp. 2267–2336, Oct. 2005.
[4] D. L. Smith and C. Mailhiot, "Proposal for strained type II superlattice infrared detectors," *J. Appl. Phys.*, vol. 62, no. 6, pp. 2545–2548, Sep. 1987.
[5] C. H. Grein, M. E. Flatte, J. T. Olesberg, S. A. Anson, L. Zhang, and T. F. Boggess, "Auger recombination in narrow-gap semiconductor superlattices incorporating antimony," *J. Appl. Phys.*, vol. 92, no. 12, pp. 7311–7316, Dec. 2002.
[6] R. Rehm, M. Walther, J. Fleibner, J. Schmitz, J. Ziegler, W. Cabanski, and R. Breiter, "Bispectral thermal imaging with quantum-well infrared photodetectors and InAs/GaSb type-II superlattices," *Proc. SPIE*, vol. 6206, pp. 62060Y-1–62060Y-11, May 2006.
[7] P. Y. Delaunay, B. M. Nguyen, D. Hoffman, A. Hood, E. K. Huang, M. Razeghi, and M. Z. Tidrow, "High quantum efficiency two color type-II InAs/GaSb n-i-p-p-i-n photodiodes," *Appl. Phys. Lett.*, vol. 92, no. 11, pp. 111 112–111 114, Mar. 2008.
[8] A. Khoshakhlagh, J. Rodriguez, E. Plis, G. D. Bishop, Y. D. Sharma, H. S. Kim, L. R. Dawson, and S. Krishna, "Bias dependent dual band response from InAs/Ga(In)Sb type II strain layer superlattice detectors," *Appl. Phys. Lett.*, vol. 91, no. 26, pp. 263 504–263 506, Dec. 2007.
[9] E. Plis, S. S. Krishna, E. P. Smith, S. Johnson, and S. Krishna, "Voltage controllable dual-band response from InAs/GaSb strained layer superlattice detectors with nBn design," *Electron Lett*, vol. 47, no. 2, pp. 133–134, Jan. 2011.
[10] G. C. Dente and M. L. Tilton, "Pseudopotential methods for superlattices: Applications to mid-infrared semiconductor lasers," *J. Appl. Phys.*, vol. 86, no. 3, pp. 1420–1429, Aug. 1999.
[11] SENTAURUS Device User Guide, Version C-2009.06, 2009. [Online]. Available: http://www.synopsys.com/Tools/TCAD/Pages/default.aspx
[12] H. S. Kim, E. Plis, N. Gautam, S. Myers, Y. Sharma, L. R. Dawson, and S. Krishna, "Reduction of surface leakage current in InAs/GaSb strained layer long wavelength superlattice detectors using SU-8 passivation," *Appl Phys. Lett.*, vol. 97, no. 14, pp. 143 512–142 514, Oct. 2010.
[13] Q. K. Yang, F. Fuchs, J. Schmitz, and W. Pletschen, "Investigation of trap-assisted tunneling current in InAs/(GaIn)Sb superlattice long-wavelength photodiodes," *Appl. Phys. Lett.*, vol. 81, no. 25, pp. 4757–4759, Dec. 2002.
[14] E. Smith, L. Pham, G. M. Venzor, E. M. Norton, M. D. Newton, P. M. Goetz, V. K. Randall, A. M. Gallagher, G. K. Pierce, E. A. Patten, R. A. Coussa, K. Kosai, W. A. Radford, L. M. Giegerich, J. M. Edwards, S. M. Johnson, S. T. Baur, J. A. Roth, B. Nosho, T. J. D. Lyon, J. E. Jensen, and R. E. Longshore, "HgCdTe focal plane arrays for dual-color mid- and long-wavelength infrared detection," *J. Electron. Mater.*, vol. 33, no. 6, pp. 509–516, Jun. 2004.
[15] W. E. Tennant, M. Thomas, L. J. Kozlowski, W. V. McLevige, D. D. Edwall, M. Zandian, K. Spariosu, G. Hildebrandt, V. Gil, P. Ely, M. Muzilla, A. Stoltz, and J. H. Dinan, "A novel simultaneous unipolar multispectral integrated technology approach for HgCdTe IR detectors and focal plane arrays," *J. Electron. Mater.*, vol. 30, no. 6, pp. 590–594, Jun. 2001.
[16] Y. Arslan, S. U. Eker, M. Kaldirim, and C. Besikci, "Large format voltage tunable dual-band QWIP FPAs," *Inf. Phys. Technol.*, vol. 52, no. 6, pp. 399–402, Nov. 2009.
[17] S. Gunapala, "Demonstration of first megapixel dual-band QWIP focal plane array," in *Proc. QSIP Conf. Present.*, 2009.
[18] G. Ariyawansa, Y. Aytac, A. G. U. Perera, S. G. Matsik, M. Buchanan, Z. R. Wasilewski, and H. C. Liu, "Five-band bias-selectable integrated quantum well detector in an *n–p–n* architecture," *Appl Phys. Lett.*, vol. 97, no. 23, pp. 231 102–231 104, Dec. 2010.